Breakdown of ergodic behavior in the Lorentz gas

James Lloyd, Lamberto Rondoni, and Gary P. Morriss
School of Physics, University of New South Wales, PO Box 1, Kensington NSW 2033, Australia
(Received 29 April 1994)

Applying an external field to the Lorentz gas model, and thermostating it to maintain a constant kinetic energy, we study the conductivity as a function of the field. For small fields the system is ergodic and the diffusion coefficient is well defined. At larger values of the field, ergodic behavior disappears and we observe a variety of possible dynamics, including the existence of a single stable trajectory for the largest fields. At intermediate values of field a series of transitions between ergodic, periodic, and nonergodic behavior appears. We present a detailed dynamical study of the breakdown in ergodic behavior.

PACS number(s): 05.45.+b

I. INTRODUCTION

There has been a recent increase in interest in the study of the Lorentz gas model originally proposed in 1905 [1]. Much of this interest has been due to the use of this model as a test case for the study of periodic orbit expansions and the Ruelle ζ-function based cycle expansions [2–5]. However, there is still much interest in understanding this simple nontrivial model from a fundamental statistical mechanical point of view. The model dynamics is completely reversible, yet the system displays irreversible behavior with a well defined diffusion coefficient. Under the application of a small external field and thermostat, the Lorentz gas has a steady average current, and the ratio of this current to the applied field is equal to the diffusion coefficient in the small field limit. These results are essentially numerical observations. The only rigorous mathematical result is that starting from any initial density, absolutely continuous with respect to the Liouville measure [e.g., $f(\mathbf{q},\mathbf{p})d\mathbf{q}\,d\mathbf{p}$, where f is an integrable function], a unique stationary, multifractal, ergodic measure is approached as time goes to infinity [6]. This result holds for small enough external fields while, at larger fields, a loss of ergodicity is expected; as yet, there has been no quantitative estimate of the value of the field at which the transition from ergodic to nonergodic behavior occurs. To establish a breakdown of ergodicity we require that there exist at least two disjoint regions, of positive Lebesgue measure, such that an initial condition in one region can never evolve dynamically to the other (even under the action of periodic boundary conditions). In this case, in fact, the natural measure of the system is decomposable, i.e., nonergodic. If the system is ergodic, ensemble averages taken over the accessible phase space in the stationary state equal time averages for almost all trajectories. This happens, for instance, when almost all initial conditions in phase space evolve towards the same attractor. For the Galton board there is some numerical evidence to suggest the existence of stable cycles of 20 or fewer collisions at large fields [7], but no systematic studies exist. Moreover, the existence of stable cycles does not necessarily imply a breakdown of ergodicity, as such orbits could be the only attractors in the phase space, thus verifying the ergodic hypothesis. This is the case, indeed, in our model for large enough values of the external field.

The modified Lorentz gas (with regularly arranged scatterers) consists of an infinite two-dimensional triangular lattice of hard scatterers with a single point particle *wandering* through the lattice. The *wandering* particle experiences simple hard core collisions with the scatterers as it moves. In the absence of a field the energy and the kinetic energy are constants of motion. As a result the speed of the wandering particle is constant, so the momentum has only one degree of freedom: its direction. Therefore we can write $\mathbf{p}=(p_x,p_y)=p(\cos\theta,\sin\theta)$ where θ is the angle between the x axis and the momentum vector. If no external field is applied, the trajectory of the wandering particle consists of straight segments of line. It is more convenient to represent the position in polar coordinates, so $(x,y)=r(\cos\phi,\sin\phi)$. (See Fig. 1.) The thermodynamic state point of the Lorentz gas has been characterized in terms of the disk spacing w, so if d is the distance between the centers, then $w=d-2\sigma$. In what follows we take the radius $\sigma=1$. For a range of values of the spacing, the Lorentz gas has an infinite horizon (that is, for some initial conditions it is possible to pass through the whole lattice without a collision). To avoid the subsequent difficulties with the definition of the diffusion coefficient we choose the spacing sufficiently small so that the horizon is finite, that is, $w\le 4/\sqrt{3}-2$. Here we shall consider the spacing $w=0.236\,068\,5$, which has been studied previously [3,5,7].

The equations of motion for the Lorentz gas in an applied external field f_e in the x direction with an isokinetic thermostat are given by

$$\begin{aligned}\dot{x}&=p_x,\quad \dot{p}_x=F_x-f_e-\alpha p_x\ ,\\ \dot{y}&=p_y,\quad \dot{p}_y=F_y-\alpha p_y\ .\end{aligned}\tag{1}$$

As the speed p of the wandering particle in the Lorentz gas is unity, and we take its mass M, to be unity, then the isokinetic temperature is given by $kT=1$ (in the limit of vanishing field, the kinetic energy equals the total energy). For the constraint of constant kinetic energy we find that

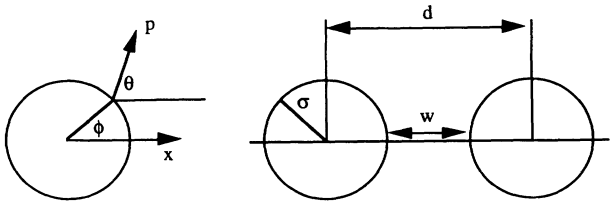

FIG. 1. The geometry of the Lorentz gas. For the scatterer at collision, the polar angle ϕ gives the position, while θ gives the angle between the momentum vector and the x axis. The system is parametrized by the ratio w/σ, where w is the spacing between scatterers.

$$\alpha=\frac{\mathbf{p}\cdot\mathbf{F}-f_e p_x}{p^2} .$$

Changing to polar coordinates we find that

$$\dot{\theta}=\varepsilon\sin\theta, \quad \text{where } \varepsilon=f_e/p . \tag{2}$$

Integrating the equation of motion for θ, we find that in time t, θ_0 evolves to θ_1 where

$$\tan(\theta_1/2)=\tan(\theta_0/2)e^{\varepsilon t} . \tag{3}$$

Integrating the equations of motion for the coordinates we find that in the same time, the changes in x and y are given by

$$x_1-x_0=\frac{p}{M\varepsilon}\ln\left[\frac{\sin\theta_1}{\sin\theta_0}\right] \quad \text{and} \quad y_1-y_0=\frac{p(\theta_1-\theta_0)}{M\varepsilon} . \tag{4}$$

In this study, we take the direction of the field to be parallel to the x axis, and the x axis to be parallel to one of the vectors joining nearest neighbors in the triangular lattice. This differs from some previous work [3,7] where the x axis was taken to be parallel to the vector joining second nearest neighbors.

II. THE BIFURCATION DIAGRAM

The Lorentz gas can be considered as a mapping rather than a continuous flow, by considering the elementary cell (the hexagon surrounding the central scatterer) and choosing the surface of the scatterer as the Poincaré surface of section. A point on the Poincaré surface is uniquely defined by specifying (ϕ,θ). A trajectory of n collisions is equivalent to specifying the values of (ϕ,θ) at each of the collisions. The mapping from collision to collision is

$$(\phi_{n+1},\theta_{n+1})=F(\phi_n,\theta_n) , \tag{5}$$

where F is defined implicitly by the integrated equations of motion. To characterize orbits in this model we make use of a form of symbolic dynamics, introduced previously [2,4,5]. This symbolic dynamics attaches a symbol (a number between 0 and 11) to each free flight of a trajectory. Each even number represents a free flight to a nearest neighbor, while an odd number is a flight to a second nearest neighbor. The labels are ordered counterclockwise to first and second nearest neighbor scatterers beginning with 0 for the nearest neighbor scatterer on the x axis.

Here we wish to study the behavior of this mapping as a function of the applied external field. In order to visualize the behavior we can consider two projections of the mapping. These are the projections onto the ϕ axis and θ axis, respectively. We find that both projections have the same dynamical features, thus we concentrate onto the θ projection only. In particular, we observe a quite complex structure which closely resembles the bifurcation diagram of one-dimensional dynamical systems.

In Fig. 2 we present the upper half of the projection of the bifurcation diagram onto the θ axis, obtained by direct iteration of a few initial conditions, ignoring the initial transient behavior ($\approx 10^3$ collisions). The other half of this diagram is trivially obtained by reflection with respect to the $\theta=0$ line. The feature of this diagram is a series of dramatic changes in the pattern of the iterates of the mapping. For fields of 2.1 or less the iterations of our initial condition sample most of the phase space, whereas at fields of 2.64 the iterations settle onto a stable orbit of length 2 (collisions) with symbol string (4 8), shown in Fig. 3. With increasing field the curvature of the orbit increases, and the orbit has multiple bounces on each scatterer, eventually approaching an orbit very similar to the *creeping-flow* trajectory observed in a related model [8], which is made of horizontal straight lines and arcs of circumference. It is interesting to note that the diffusion coefficient—as given in Ref. [3]—converges to zero in

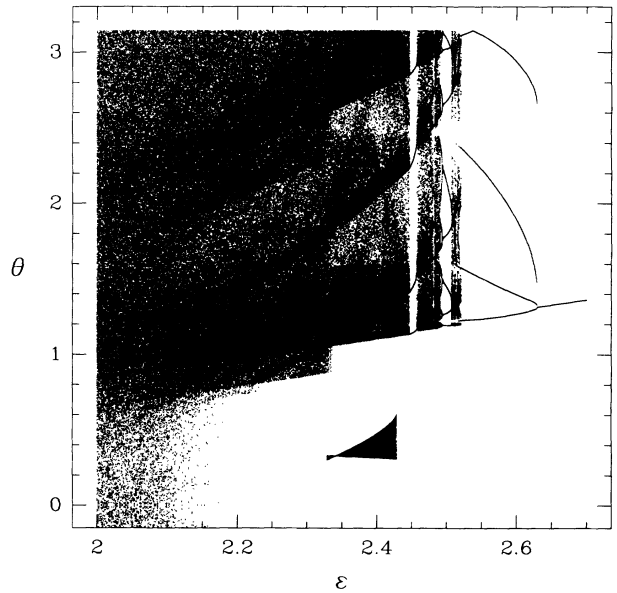

FIG. 2. The upper half of the bifurcation diagram for the discrete mapping $F(\phi,\theta)$ as a function of field ε, projected onto the (ε,θ) plane. This diagram is symmetrized by mapping $(-\theta)\Longrightarrow\theta$. Above $\varepsilon=2.64$ there is a single line which is the stable (4 8) length-2 orbit, which then becomes a stable length-8 orbit. After that there are chaotic bands interspersed with periodic windows. The separated feature at $2.3<\varepsilon<2.46$ is one example of the neutrally stable elliptical orbit $(4\ 10)^{\infty}$.

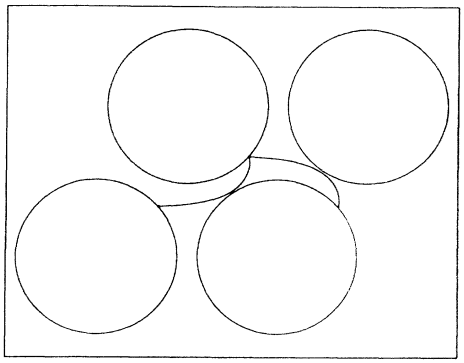

FIG. 3. The stable length-2 orbit (4 8) at $\varepsilon=2.7$. As the field is in the negative x direction, the wandering particle moves from right to left.

this limit. We now concentrate on the range of fields $2.1<\varepsilon<2.64$, where significant changes in the bifurcation diagram occur.

As the field decreases, the curvature of the orbit decreases, and the two free flights both develop zero-effect glancing collisions when $\varepsilon\approx 2.64$. Any further decrease in the field *prunes* the (4 8) orbit (in the sense that it is not physically realizable). As the scatterer surfaces are convex (hence defocusing), each additional collision introduces more instability into the orbit, because close points tend to diverge from each other more and more at every collision event. So a transition from a length-2 to a, say, length-4 orbit is likely to produce a markedly more unstable orbit. What actually happens in our Lorentz gas model is that dynamical stability favors introducing as few as possible new collisions per free flight, so that the new stable orbit, which emerges from reducing the field to values slightly below 2.64, consists of taking three sequential copies of the original length-2 orbit and introducing only two extra collisions. The length-8 orbit so formed is the most stable possible structure [see Fig. 4(b)], which is obtained by introducing on average only $\frac{1}{3}$ of a collision per single free flight of the old length-2 orbit. Such a length-8 orbit consists of four free flights, followed by the mirror image (in the x axis) of the same four free flights. [See Figs. 4(a) and 4(b).]

In the bifurcation diagram (Fig. 2), this information is expressed by the fact that each of the original two points of the stable (4 8) orbit splits into three different points, while two new points are generated, as the field is lowered from higher to smaller values than 2.64. This breaks the symmetry of the orbit obtained by pasting together three copies of the original (4 8). The two new points that emerge represent the two new collisions, they lie on the two new lines which start at a field of about 2.64 not branching from any other line. Clearly, although the bifurcation diagram in Fig. 2 seems reminiscent of those for one-dimensional maps, the mechanism at work is quite different. As the field is decreased, the free flights of the stable length-8 orbit become less curved, eventually intersect a scatterer, and the orbit is pruned. The stability of the orbit decreases continuously as the field is lowered

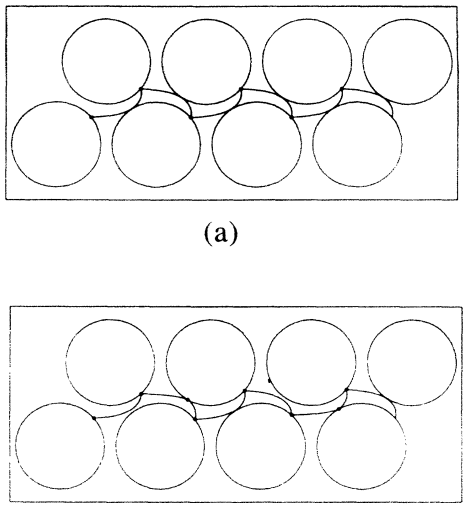

FIG. 4. Three copies of the stable length-2 orbit (4 8) just before it is pruned at $\varepsilon=2.64$. If the field is decreased further, the curved part intersects the scatterer. (b) The same as (a) except that the field has been reduced further, $\varepsilon=2.625$, and the stable length-2 orbit has been pruned. It is replaced by a stable length-8 orbit (2 6 8 4 10 6 4 8) which is similar to the three copies of (4 8) but has two extra collisions.

from values close to the pruning point, and at a field slightly above the pruning value, the orbit turns unstable. At this point the dynamical system adopts the next most stable behavior, which could be another regular orbit or a chaotic one.

However, some interesting phenomena take place be-

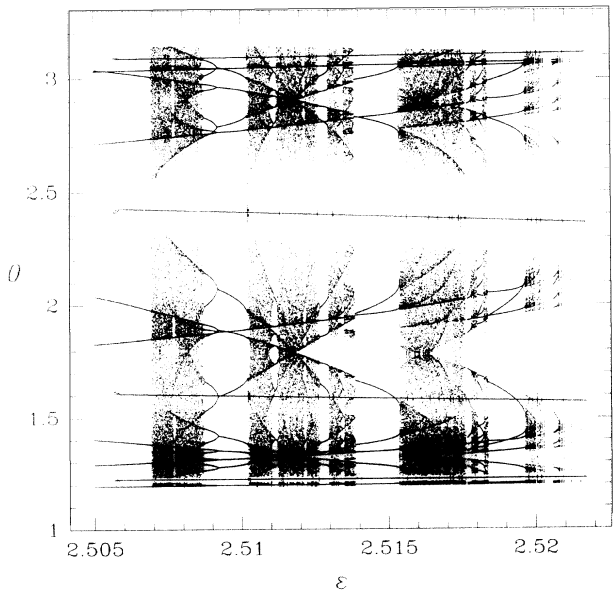

FIG. 5. A very complicated structure of chaotic bands and interspersed periodic windows containing further bifurcations. Because of the small magnitude of the Lyapunov exponents in the chaotic bands it is not possible to eliminate the possibility that these are long *chaotic* transients.

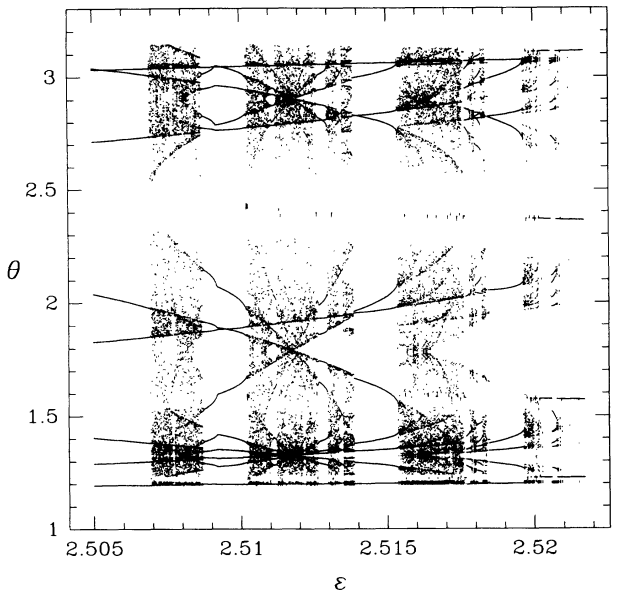

FIG. 6. A version of Fig. 5, where only one initial condition is used at each value of the field. This shows that the false bifurcation at $\varepsilon=2.509$ is a transition from a symmetric length-28 orbit to two asymmetric length-28 orbits. Using only one initial condition we obtain only one of the asymmetric orbits, thus the bifurcation appears to be *one sided.*

fore the length-8 orbit is pruned. In particular, an enlargement of the range $2.505<\varepsilon<2.522$ reveals a very complex structure made of several different chaotic regions separated by macroscopic ranges of periodic dynamics, and finely interspersed with periodic windows of small, as well as large, periods (Fig. 5). For values of the field in this region, and smaller, there is a clear window of regular behavior ($2.49<\varepsilon<2.507$) which begins with a symmetric stable cycle of length 16. The next change in behavior would appear to be a bifurcation to a cycle of length 32, at about 2.495. However, closer examination reveals that the relevant points in phase space really refer to two distinct, asymmetric cycles of length 16. The one we observe depends upon the initial condition. Thus we have a *false bifurcation,* through which the period of the orbits remains unchanged, while their number doubles. The same happens at $\varepsilon\approx2.5092$, and Fig. 6 shows what Fig. 5 would look like if only one initial condition is used at each value of the field. (A more complete description of the behavior of the system will be published elsewhere [9].)

III. THE ORBITS

To understand the bifurcation diagram at fields smaller than those considered in Sec. II, it is helpful to consider the behavior of some of the shortest orbits. The simplest are the short-flight orbits of length 2. The orbit (0 6) is unstable, and as it is parallel to the field its shape is unchanged with increasing field. The (4 10) orbit, however, does change in shape and stability, with increasing field. Both of the collisions in this orbit are normal (i.e., $\theta=\phi\pm\pi$) so the orbit can be completely characterized by the knowledge of two angles only. The (4 10) orbit is unstable for fields in the range $0\le\varepsilon<2.46$, but for values in $2.3<\varepsilon<2.46$ there is a second initial condition which gives rise to a different (4 10) orbit with vanishing Lyapunov exponent. Around this point there is a continuum of initial conditions each of which begins a distinct orbit in phase space, whose collision points fill up a distinct ellipse when drawn in the (ϕ,θ) plane (see Fig. 7). The presence of elliptic rather than hyperbolic trajectories, in phase space, shows that there are values of the field for which the hyperbolicity properties of the Lorentz gas are lost. Moreover, we observe that all of these elliptic orbits have symbol string $(4\ 10)^{\infty}$ where the superscript stresses that the same symbol sequence is repeated indefinitely without closing. This illustrates two features of the model at such fields. First, a single symbol string (in the usual 12-symbolic dynamics) does not necessarily correspond to a unique orbit. Moreover, the problem cannot be solved by partitioning the surface of the scatterers into a finite number of pieces, and assigning a different symbol to each piece. Indeed, for a symbolic dynamics to be able to assign a single orbit to a given symbol, in this case it is necessary to have infinitely many partitions and infinitely many symbols. The second interesting feature is that the behavior of an orbit is strongly dependent on the initial condition, which leads to loss of ergodicity. Indeed, we see in Fig. 7 that the fraction of phase space covered by elliptic orbits has positive Lebes-

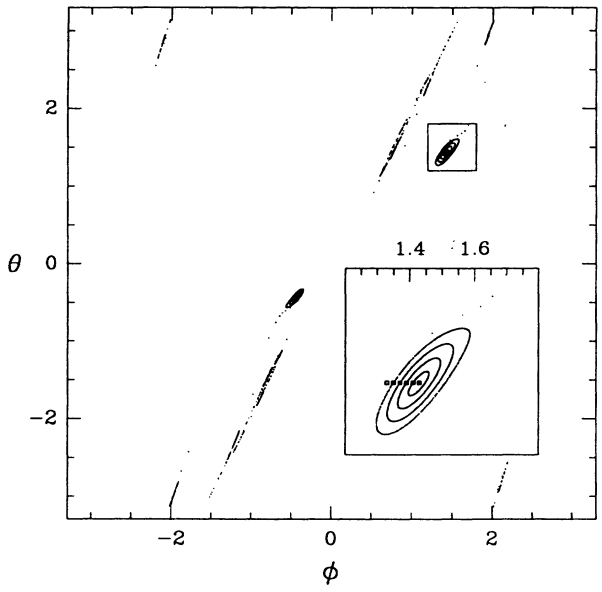

FIG. 7. A plot of the full (ϕ,θ) plane at $\varepsilon=2.43$ for a series of initial conditions near the neutrally stable (4 10) orbit. Around this point there is a continuum of initial conditions, each of which produces a distinct neutrally stable elliptical orbit $(4\ 10)^{\infty}$, centered about the neutrally stable (4 10) orbit. In the inset, the small squares represent the initial conditions, while the other points represent their time evolution. Five of the initial conditions give elliptical orbits while the outer one gives a chaotic orbit.

gue measure, and that the orbits starting outside that region eventually settle down on what appears to be a chaotic attractor. Thus $\varepsilon=2.3$ is an upper bound for ergodicity.

In Fig. 7 there should also be elliptical orbits from the symmetry related $(2\ 8)^{\infty}$ orbit. These extra (ϕ,θ) plane contributions will be the same as those from the $(4\ 10)^{\infty}$ orbit reflected in the line $\theta=-\phi$, however, their regions of existence are disjoint, and do not overlap with the basin of attraction of the chaotic orbit. Figure 8 is a plot of the possible initial conditions for the length-2 (4 10) orbit as a function of the field. On the upper branch of the curve, $1.575<\phi_0<2\pi/3$, there are the initial conditions which lead to unstable orbits, while the lower branch of the curve, $1.2<\phi_0<1.575$, leads to neutrally stable orbits. For $2.3<\varepsilon<2.46$ a region of coexistence occurs where both unstable and neutrally stable orbits are possible. Figure 9 shows the unstable, and the stable (4 10) orbit, along with the critical angle at which the two orbits coincide. It is interesting to note that the orbit disappears at a field of 2.46, not because it intersects a scatterer, but because there are no solutions to the trajectory equations consistent with normal collisions at each scatterer. We refer to this as *orbit disappearance.*

Another region where ergodicity is lost is for values of the field between 2.5061 and 2.507, where stable orbits of length 8 and length 16 coexist. Thus whether the long time evolution of a given point in phase space will be captured by the one or the other orbit depends upon the initial condition. Again, the natural measure can be decomposed in at least two ergodic measures, and it cannot itself be ergodic. Also, around $\varepsilon\approx 2.506\,09$, the stability of the length-8 orbit changes, as its Lyapunov number grows from negative to positive values continuously as a function of the field. This orbit remains unstable until the field is so small that two of its free flights intersect a scatterer, and the orbit is pruned.

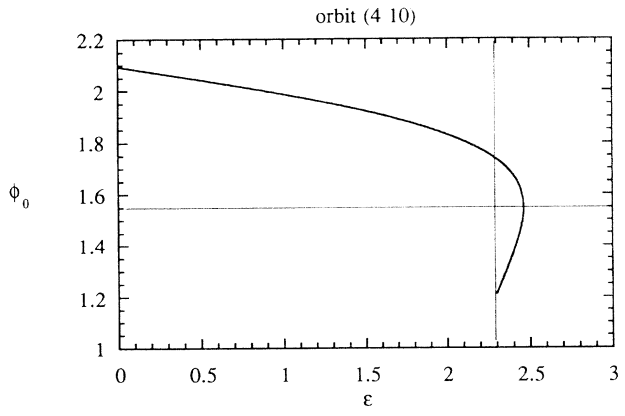

FIG. 8. The possible initial conditions for (4 10) orbits as a function of ε. For $\varepsilon<2.3$ there is a single unstable initial condition. For $2.3<\varepsilon<2.46$ there are two initial conditions, the upper one unstable and the lower one neutrally stable.

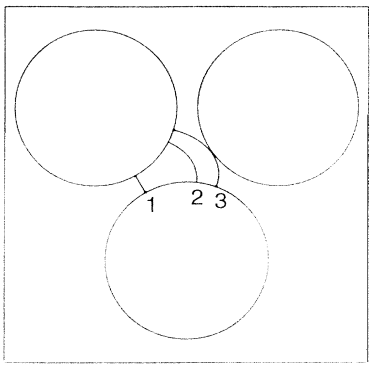

FIG. 9. The full range of possible (4 10) orbits as a function of ε. The orbit marked (1) is the $\varepsilon=0$ orbit; the orbit marked (2) is the limiting unstable orbit at $\varepsilon=2.46$; and the orbit marked (3) is the small field limit for the neutrally stable orbit at $\varepsilon=2.3$. Any (4 10) orbit between (1) and (2) is unstable and moves to the right with increasing field, while any orbit between (2) and (3) is neutrally stable and moves to the left with increasing field.

IV. CONCLUSIONS

In summary we have seen four mechanisms that lead to changes in the bifurcation diagram with changes in the value of the field, not all of which have been found before in maps of the interval; (1) change in the stability of an orbit (the length-8 orbit at $\varepsilon\approx 2.506\,09$), (2) pruning of an orbit by a scatterer (length-2 goes into length-8 orbit), (3) disappearance of an orbit (the (4 10) at $\varepsilon\approx 2.48$], and (4) orbit doubling (the bifurcation with no change in period at $\varepsilon\approx 2.5092$). It is interesting to note that the stability of a given orbit usually decreases as the field is moved in the direction of pruning of the orbit. However, in general, it is not the case that an orbit is pruned when it changes its stability. In the bifurcation diagram of the quadratic map only the first of the four mechanisms described above is evident. The last two mechanisms seem to be peculiar to the underlying dynamics of the Lorentz gas. However, as pruning is observed also in other sorts of symbolic dynamic systems, it is possible that features similar to those caused by pruning in the Lorentz gas are shared by two-dimensional maps.

We have shown that ergodicity is lost when $2.3<\varepsilon<2.46$, because the (ϕ,θ) plane is composed of a chaotic region, and two pairs of elliptical regions consisting of infinitely many neutrally stable orbits, $(4\ 10)^{\infty}$ and $(2\ 8)^{\infty}$. In this case the measure is decomposable into at least three regions. Ergodicity is also lost at every false bifurcation (or orbit doubling) of stable orbits, like those discussed in Sec. II, because the measure is once again decomposable.

A very detailed study of a Galton-board model similar to ours has been recently published [10], where questions

about ergodicity and the existence of chaotic as well periodic attractors have been addressed. The main differences are that in their model they consider inelastic collisions, and there is no thermostating mechanism to remove work done by gravity. Although it is difficult to justify the use of a thermostat in the Galton board [10], the absence of such a mechanism makes it much more difficult to establish a stationary state.

[1] H. A. Lorentz, Proc. Amst. Acad. **7**, 438 (1905).
[2] P. Cvitanovic, P. Gaspard, and T. Schreiber, Chaos **2**, 85 (1992).
[3] W. N. Vance, Phys. Rev. Lett. **69**, 1356 (1992).
[4] P. Cvitanovic, J-P. Eckmann, and P. Gaspard, Chaos, Solitons Fractals (to be published).
[5] G. P. Morris and L. Rondoni, J. Stat. Phys. **75**, 553 (1994).
[6] N. I. Chernov, G. L. Eyink, J. L. Lebowitz, and Ya. G. Sinai, Phys. Rev. Lett. **70**, 220 (1993); Commun. Math. Phys. **154**, 569 (1993).
[7] B. Moran and W. G. Hoover, J. Stat. Phys. **48**, 709 (1987).
[8] W. G. Hoover and B. Moran, Chaos **2**, 599 (1992).
[9] J. Lloyd, M. Niemeyer, L. Rondoni, and G. P. Morriss (unpublished).
[10] A. Lue and H. Brenner, Phys. Rev. E **47**, 3128 (1993).

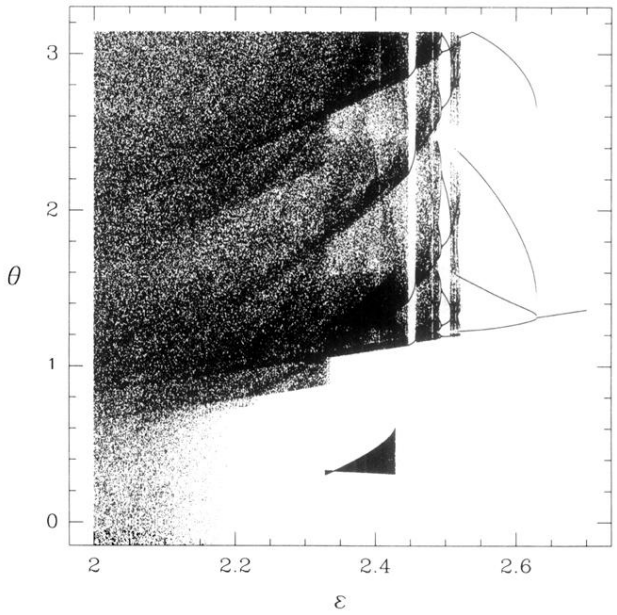

FIG. 2. The upper half of the bifurcation diagram for the discrete mapping $F(\phi,\theta)$ as a function of field ε, projected onto the (ε,θ) plane. This diagram is symmetrized by mapping $(-\theta)\Longrightarrow\theta$. Above $\varepsilon=2.64$ there is a single line which is the stable (4 8) length-2 orbit, which then becomes a stable length-8 orbit. After that there are chaotic bands interspersed with periodic windows. The separated feature at $2.3<\varepsilon<2.46$ is one example of the neutrally stable elliptical orbit $(4\ 10)^{\infty}$.

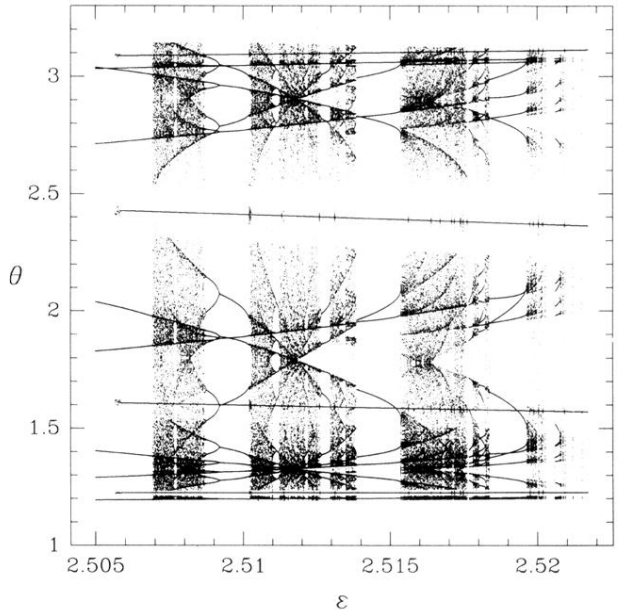

FIG. 5. A very complicated structure of chaotic bands and interspersed periodic windows containing further bifurcations. Because of the small magnitude of the Lyapunov exponents in the chaotic bands it is not possible to eliminate the possibility that these are long *chaotic* transients.

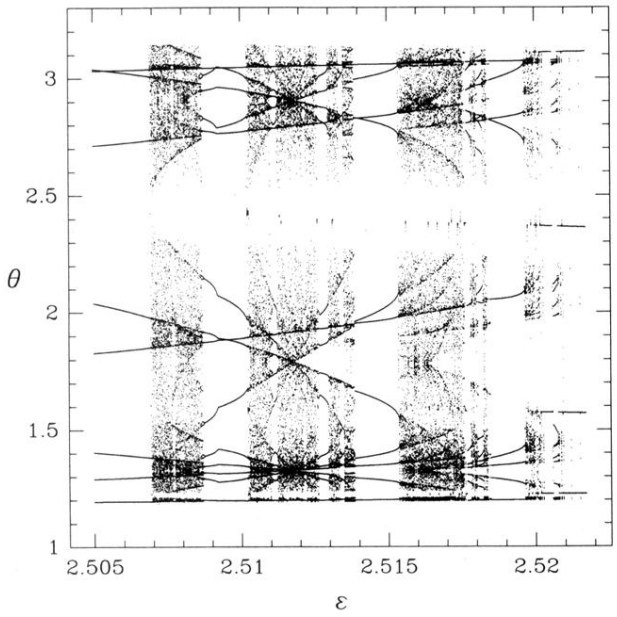

FIG. 6. A version of Fig. 5, where only one initial condition is used at each value of the field. This shows that the false bifurcation at $\varepsilon=2.509$ is a transition from a symmetric length-28 orbit to two asymmetric length-28 orbits. Using only one initial condition we obtain only one of the asymmetric orbits, thus the bifurcation appears to be *one sided.*